Safety-Critical Predictive Control for Dynamic Visual Servoing of Robot Manipulators With Visibility Constraints

Xinyi Jiang[1], Jianliang Mao[1], Yunda Yan[2], Linyan Han[3], and Chuanlin Zhang[1]

***Abstract*— This paper addresses the challenges of view constraints in image-based visual servoing systems for tracking dynamic targets. The unknown trajectory of moving targets poses significant challenges to tracking systems, particularly when targets move outside the camera's field of view or encounter occlusions, potentially leading to ineffective control signals and safety risks. To address these issues, this paper proposes a safety-critical predictive control methodology based on robust control barrier functions. First, a predictive controller is designed to achieve rapid and unbiased tracking while reducing computational load. Then, a non-linear optimization problem is formulated by combining robust control barrier functions. Finally, simulation experiments validate the proposed approach. The results demonstrate that the method not only exhibits favorable dynamic performance in disturbance-free environments but also maintains effectiveness under interference conditions. The solution effectively addresses visual servo target visibility issues, significantly enhances computational efficiency, and demonstrates promising potential for engineering applications.**

I. INTRODUCTION

Visual servoing, as a technology achieving precise control through visual feedback in dynamic environments, plays an indispensable role in robotic control due to its accuracy and flexibility [1], [2]. According to implementation paradigms, visual servoing systems are generally classified into three categories [3]: position-based visual servoing (PBVS), image-based visual servoing (IBVS), and hybrid approaches. IBVS specifically utilizes geometric features on the image plane (e.g., points, lines, or line segments) to design controllers through the image Jacobian matrix, typically employing proportional control schemes [4]. This methodology demonstrates strong robustness against camera calibration errors and model inaccuracies while maintaining high control precision, as it eliminates the need for calibrating the relative pose between end-effectors and target objects [5].

A critical challenge in visual servoing emerges when targets move outside the camera's field of view (FOV) or experience occlusion, potentially leading to control signal interruptions and safety hazards [6], [7]. Model predictive control (MPC) has gained prominence in visual servoing applications due to its constraint-handling capability and predictive optimization of control sequences [8], [9]. However, dynamic target tracking introduces multiple disturbances including target motion uncertainty, sensor noise, and model discrepancies, which significantly degrade tracking performance [10]. Robust MPC variants have been developed to enhance disturbance rejection in uncalibrated visual servoing systems operating under constrained environments [10], [11]. Nevertheless, the inherent computational complexity of MPC implementations may compromise real-time responsiveness, limiting their practical deployment. The MPC approach addresses this issue through offline prediction model optimization via successive Taylor expansions, effectively reducing computational overhead [12]. However, its inability to handle constraint satisfaction imposes practical limitations.

Recent advancements in control barrier function (CBF) theory have established it as a powerful framework for addressing nonlinear system constraints [13]. The principal strength of CBF lies in its compatibility with conventional feedback controllers or control Lyapunov functions through quadratic programming formulations, enabling simultaneous preservation of system safety and control performance. Applications in visual servoing have emerged, such as the integration of MPC with CBF to prevent target occlusion [14], [15]. Nevertheless, standard CBF implementations require precise model knowledge, presenting challenges when applied to disturbance-affected systems [16].

Building upon these foundations, this paper proposes a safe IBVS control framework incorporating robust control barrier functions. The methodology comprises three key innovations: First, a nominal predictive controller is designed for precise dynamic target tracking. Second, a disturbance observer-integrated robust CBF is developed to guarantee instantaneous safety under perturbed conditions. Finally, an optimization framework synergistically combines the nominal controller with the robust CBF, achieving balanced consideration of tracking performance and safety constraints. This integrated approach provides an efficient and reliable solution for dynamic target visual servoing applications.

II. MATHEMATICAL MODEL AND CONTROL OBJECTIVE

A. Visual Servoing Kinematic Modeling

Consider a robotic system composed of a six-degree-of-freedom (6-DOF) manipulator, equipped with a camera mounted at its end-effector. The camera coordinate frame $\mathscr{F}_c$ is defined such that the Z-axis aligns with the optical axis, and its origin coincides with the principal point of the image sensor.

*This work was supported in part by the National Natural Science Foundation of China under Grant 62203292. (*Corresponding author: Jianliang Mao.*)

[1]Xinyi Jiang, Jianliang Mao, and Chuanlin Zhang are with College of Automation Engineering, Shanghai University of Electric Power, Shanghai, China. xinyi_jiang@mail.shiep.edu.cn, jl_mao@shiep.edu.cn, clzhang@shiep.edu.cn

[2]Yunda Yan is with Department of Computer Science, University College London, London, U.K. e-mail: yunda.yan@ucl.ac.uk

[3]Linyan Han is with School of Mechanical Engineering, University of Leeds, Leeds, U.K. e-mail: l.y.han@leeds.ac.uk

Let $\boldsymbol{P}_i = [X_i, Y_i, Z_i]^T$, $i = 1, \ldots, m$, denote a set of m static 3D points represented in the camera frame. Their corresponding 2D image projections are given by $\boldsymbol{s}_i = [u_i, v_i]^T$, and are computed as

$$\boldsymbol{s}_i = \begin{bmatrix} u_i \\ v_i \end{bmatrix} = \frac{\lambda}{Z_i} \begin{bmatrix} X_i \\ Y_i \end{bmatrix} \tag{1}$$

where λ denotes the camera's focal length in pixels.

The camera's spatial velocity is defined as $\boldsymbol{v}_c = (\boldsymbol{v}_c^c, \boldsymbol{\omega}_c^c)$, with $\boldsymbol{v}_c^c$ and $\boldsymbol{\omega}_c^c$ representing translational and angular velocities, respectively. The time derivative of the image feature coordinates $\boldsymbol{s}_i$ is related to the camera motion through

$$\dot{\boldsymbol{s}}_i = \boldsymbol{L}_{s_i} \boldsymbol{v}_c \tag{2}$$

where $\boldsymbol{L}_{s_i}$ is the interaction matrix associated with the i-th feature, describing how image motion is induced by camera velocity. Its analytical form is given by

$$\boldsymbol{L}_{s_i} = \begin{bmatrix} -\frac{\lambda}{Z_i} & 0 & \frac{u_i}{Z_i} & \frac{u_i v_i}{\lambda} & -\frac{\lambda^2+v_i^2}{\lambda} & v_i \\ 0 & -\frac{\lambda}{Z_i} & \frac{v_i}{Z_i} & \frac{\lambda^2+v_i^2}{\lambda} & -\frac{u_i v_i}{\lambda} & -u_i \end{bmatrix} \tag{3}$$

where Z_i is the depth of the i-th point in frame $\mathscr{F}_c$. The matrix $\boldsymbol{L}_{s_i}$ can be decomposed into components for translational and rotational velocities as

$$\boldsymbol{L}_{i,v} = \begin{bmatrix} -\frac{\lambda}{Z_i} & 0 & \frac{u_i}{Z_i} \\ 0 & -\frac{\lambda}{Z_i} & \frac{v_i}{Z_i} \end{bmatrix}, \quad \boldsymbol{L}_{i,\omega} = \begin{bmatrix} \frac{u_i v_i}{\lambda} & -\frac{\lambda^2+v_i^2}{\lambda} & v_i \\ \frac{\lambda^2+v_i^2}{\lambda} & -\frac{u_i v_i}{\lambda} & -u_i \end{bmatrix} \tag{4}$$

Define the tracking error vector as $\boldsymbol{e} = [\boldsymbol{e}_1^T(t), \boldsymbol{e}_2^T(t), \ldots, \boldsymbol{e}_m^T(t)]^T$, where

$$\boldsymbol{e}_i(t) = \boldsymbol{s}_i(t) - \boldsymbol{s}_{d_i}, \quad i = 1, 2, \ldots, m \tag{5}$$

and $\boldsymbol{s}_{d_i}$ denotes the desired 2D image coordinates of the i-th feature point.

B. Control Barrier Function

Control barrier functions (CBFs) provide a systematic and mathematically rigorous mechanism for encoding safety constraints into nonlinear control systems. These functions enable the construction of forward-invariant sets, ensuring that once the system's state enters a designated safe set, it remains within that set for all future time.

Consider a general class of control-affine nonlinear systems described by the following dynamical equation:

$$\dot{x} = f(x) + g(x)u, \tag{6}$$

where $x \in \mathbb{R}^n$ denotes the system state vector, $u \in \mathbb{R}^m$ represents the control input, and the mappings $f : \mathbb{R}^n \to \mathbb{R}^n$ and $g : \mathbb{R}^n \times \mathbb{R}^m \to \mathbb{R}^{n \times m}$ are assumed to be locally Lipschitz continuous over $\mathbb{R}^n$. This structure is commonly encountered in many robotic and control applications due to its generality and analytical tractability.

To formulate safety constraints, let us define a continuously differentiable scalar function $h(x) : \mathbb{R}^n \to \mathbb{R}$, which characterizes a desired safe region in the state space. Specifically, the safe set $\mathscr{C} \subseteq \mathbb{R}^n$ associated with $h(x)$ is constructed as:

$$\begin{aligned} \mathscr{C} &= \{x \in \mathbb{R}^n : h(x) \geq 0\}, \\ \partial\mathscr{C} &= \{x \in \mathbb{R}^n : h(x) = 0\}, \\ \mathrm{Int}(\mathscr{C}) &= \{x \in \mathbb{R}^n : h(x) > 0\}, \end{aligned} \tag{7}$$

where $\mathscr{C}$ denotes the set of all states satisfying the safety criterion, $\partial\mathscr{C}$ its boundary, and $\mathrm{Int}(\mathscr{C})$ its interior.

Definition 1: Let $\mathscr{C}$ be defined as the zero-superlevel set of a continuously differentiable function $h(x) : \mathbb{R}^n \to \mathbb{R}$, as specified in (7). The function $h(x)$ is said to be a *control barrier function* for the control-affine system (6) on the set $\mathscr{C}$ if, for all $x \in \mathscr{C}$, the following condition holds:

$$\sup_{u \in \mathbb{R}^m} \left[L_f h(x) + L_g h(x) u \right] \geq -\alpha(h(x)), \tag{8}$$

where $L_f h(x)$ and $L_g h(x)$ denote the Lie derivatives of $h(x)$ along the vector fields $f(x)$ and $g(x)$, respectively, and $\alpha : \mathbb{R} \to \mathbb{R}$ is a class-$\mathscr{K}$ function ensuring constraint regularity.

Lemma 1: Suppose that $h(x)$ qualifies as a control barrier function for the system (6). If there exists a control policy $u = \pi(x) \in \mathscr{U}$ such that, for every state $x \in \mathbb{R}^n$, the following inequality is satisfied:

$$L_f h(x) + L_g h(x) \pi(x) \geq -\alpha(h(x)), \tag{9}$$

then the set $\mathscr{C} = \{x \in \mathbb{R}^n : h(x) \geq 0\}$ is *forward invariant* under the closed-loop system governed by $u = \pi(x)$. That is, if the initial condition $x(0) \in \mathscr{C}$, the state trajectory $x(t)$ will remain within $\mathscr{C}$ for all future time $t \geq 0$, thereby guaranteeing the satisfaction of the specified safety constraint.

C. Control Objective

Considering tracking a dynamic target, the IBVS system can be formulated as

$$\dot{\boldsymbol{s}}_i = L_{s_i} \begin{bmatrix} \boldsymbol{v}_c^c - \boldsymbol{v}_{s_i}^c \\ \boldsymbol{\omega}_c^c \end{bmatrix} \tag{10}$$

where $\boldsymbol{v}_{s_i}^c$ is the velocity of the point expressed in the camera frame. Given that the motion trajectories of the feature points are unknown and challenging to measure, this motion is modeled as unknown disturbance, which can be estimated by disturbance observer. The dynamics of the multiple feature points $\boldsymbol{s} = [s_1, \ldots, s_m]^\top \in \mathbb{R}^{2m}$ can be expressed as

$$\dot{\boldsymbol{s}} = \boldsymbol{L}_{\boldsymbol{s}} \boldsymbol{v}_c + \boldsymbol{d} \tag{11}$$

where $\boldsymbol{L}_{\boldsymbol{s}} = [\boldsymbol{L}_{s_1}^\top, \ldots, \boldsymbol{L}_{s_m}^\top]^\top \in \mathbb{R}^{2m \times 6}$ is the overall image Jacobian matrix.

For system (11), this paper aims to design a secure controller to meet the following dual objectives:

1) Under the influence of disturbances, the system can accurately follow the reference feature positions, thereby achieving excellent dynamic tracking performance;
2) When the system is subjected to disturbances, the target is strictly maintained within the allowable field of view while achieving occlusion avoidance, to guarantee safe and reliable system operation.

III. Nominal Predictive Controller Design

A. Disturbance Observer Design

To ensure that the system can accurately track the given reference feature points under the influence of disturbances and guarantee safe operation of the system, it is crucial to estimate disturbances in the system quickly and accurately. To address this challenge, this paper constructs a disturbance observer [17], which is specifically described as

$$\begin{cases} \dot{\boldsymbol{z}}_0 = \boldsymbol{L}_s \mathbf{v}_c - k_0 |\Phi_0|^{\frac{1}{2}} \operatorname{sign}(\Phi_0) + \boldsymbol{z}_1 \\ \dot{\boldsymbol{z}}_1 = -k_1 \operatorname{sign}(\Phi_0) \\ \Phi_0 = \boldsymbol{z}_0 - \boldsymbol{s} \end{cases} \tag{12}$$

where z_1 is the estimates of d and k_i $(i = 0, 1)$ are positive gain coefficients.

B. Nominal Predictive Controller Design

Based on the disturbance estimation information obtained from the disturbance observer, the steady-state signals of the IBVS system are constructed as

$$\boldsymbol{v}_d = \boldsymbol{L}_s^{+}(\dot{\boldsymbol{s}}_d - \boldsymbol{z}_1). \tag{13}$$

Define the system errors as $\boldsymbol{e}_s = \boldsymbol{s} - \boldsymbol{s}_d$ and $\boldsymbol{e}_v = \boldsymbol{v}_c - \boldsymbol{v}_c^*$.To ensure optimal tracking performance, the following performance index is defined as

$$J(t) = \frac{1}{2} \int_0^T ||\boldsymbol{e}_s(t+\tau)||^2 \, d\tau \tag{14}$$

where T is the prediction horizon. The performance index $J(t)$ quantifies the tracking error over the prediction horizon and is crucial for optimizing the control input by minimizing the accumulated error, thereby enhancing the tracking accuracy and stability of the system. The tracking error $\boldsymbol{e}_s(t+\tau)$ over the prediction horizon $(0 \le \tau \le T)$ can be approximated using a first-order Taylor series expansion along the system dynamics, as follows:

$$\boldsymbol{e}_s(t+\tau) \approx \boldsymbol{e}_s(t) + \tau \boldsymbol{L}_s \boldsymbol{e}_v(t). \tag{15}$$

Neglecting the disturbance estimation error and substituting (15) into equation (14), letting $\partial J / \partial \boldsymbol{e}_v = 0$ and $\partial^2 J / \partial e_v^2 > 0$, the optimal control law can be obtained as $\boldsymbol{e}_v^* = -\frac{3}{2T} \boldsymbol{L}_s^{+} \boldsymbol{e}_s$. Therefore, the optimized velocity controller can be obtained by

$$\boldsymbol{v}_{\text{nom}} = -\frac{3}{2T} \boldsymbol{L}_s^{+} \boldsymbol{e}_s + \mathbf{v}_d. \tag{16}$$

IV. Safety-Critical Predictive Controller Design

A. Field-of-View Constraints Using CBFs

To keep the tracked object within the FOV constraints, the image feature points must meet the following conditions:

$$\begin{bmatrix} u_{\min} \\ v_{\min} \end{bmatrix} < \boldsymbol{s}_i < \begin{bmatrix} u_{\max} \\ v_{\max} \end{bmatrix}, \quad i = 1, 2, \ldots, n \tag{17}$$

where $u_{\min}$, $v_{\min}$ and $u_{\max}$, $v_{\max}$ specify the lowest and topmost bounds of the image plane in pixels. Control barrier functions are constructed to address the FOV constraints:

$$\begin{cases} h_1(\boldsymbol{s}) = \boldsymbol{s}_{\max} - \boldsymbol{s}, \\ h_2(\boldsymbol{s}) = \boldsymbol{s} - \boldsymbol{s}_{\min}. \end{cases} \tag{18}$$

where $\boldsymbol{s}_{\max} = [u_{\max}; v_{\max}]^T$ and $\boldsymbol{s}_{\min} = [u_{\min}; v_{\min}]^T$. Based on (18), the IBVS system's FOV constrained safety sets are constructed as

$$\Omega_i = \{\boldsymbol{s} \in \mathbb{R}^{2m} \mid h_i(\boldsymbol{s}) \ge 0\}, \quad i = 1, 2. \tag{19}$$

B. Occlusion-Free Constraints Using CBFs

In the workspace, the presence of an obstacle must be taken into account. As the camera moves, the target object may be occluded by the obstacle. To address this, the obstacle is modeled as a rigid sphere. The sphere is projected as a circle within the image plane. The center of the circle and a point in the circumference are defined as $\boldsymbol{s}_{o1} = [u_{o1}; v_{o1}]^T$ and $\boldsymbol{s}_{o2} = [u_{o2}; v_{o2}]^T$. Therefore, to avoid occlusion of the target object, the control barrier functions can be defined as

$$h_3(\boldsymbol{s}) = \|\boldsymbol{s} - \boldsymbol{s}_{o1}\|^2 - \|\boldsymbol{s}_{o2} - \boldsymbol{s}_{o1}\|^2, \tag{20}$$

and the safety set for occlusion-free states is thus defined as

$$\Omega_3 = \{\boldsymbol{s}_i \in \mathbb{R}^2 \mid h_{3i}(\boldsymbol{s}_i) \ge 0\}. \tag{21}$$

According to the literature [30], if the initial state of the system $\boldsymbol{s}(0)$ satisfies $\boldsymbol{s}(0) \in \Omega_s := \Omega_1 \cap \Omega_2 \cap \Omega_3$, then the admissible control space for Lipschitz continuous controller rendering :

$$\boldsymbol{v}_c(\boldsymbol{s}) \in \left\{\boldsymbol{v}_c \in \mathbb{R} \mid L_{g_1} h_i(\boldsymbol{s}) \boldsymbol{v}_c + L_{g_2} h_i(\boldsymbol{s}) \boldsymbol{d} + \alpha(h_i(\boldsymbol{s})) \ge 0\right\} \tag{22}$$

where $g_1 = L_{\mathbf{s}}$ and $g_2 = 1$. The state $\boldsymbol{s}(t)$ will always remain within the safe domain Ω_s. Here, α is an extended class $\mathscr{K}_\infty$ function.

C. Robust CBF Design

In practical applications of IBVS systems, the direct implementation of CBF constraints is often infeasible due to the presence of unknown disturbances. To overcome this challenge, we propose incorporating disturbance estimation into the constraint design. The original constraint can be reformulated in a practical form as

$$\begin{aligned} \boldsymbol{v}_c(\boldsymbol{s}) \in \{\boldsymbol{v}_c \in \mathbb{R} \,|\, & L_{g_1} h_i(\boldsymbol{s}) \boldsymbol{v}_c + L_{g_2} h_i(\boldsymbol{s}) \hat{\boldsymbol{d}} \\ & - L_{g_2} h_i(\boldsymbol{s})(\hat{\boldsymbol{d}} - \boldsymbol{d}) + \alpha(h_i(\boldsymbol{s})) \ge 0\}. \end{aligned} \tag{23}$$

From [18] can be seen that the compensation of the disturbance estimation error $\hat{\boldsymbol{d}} - \boldsymbol{d}$ is crucial for ensuring the safety of the system under the influence of disturbances.

Defining $\eta_0 = z_0 - s$ and $\eta_1 = z_1 - d$. According to (12) the error dynamics of the matched disturbance observer can be derived as follows:

$$\begin{cases} \dot{\eta}_0 = \eta_1 - k_0 |\eta_0|^{\frac{1}{2}} \operatorname{sign}(\eta_0), \\ \dot{\eta}_1 = -k_1 \operatorname{sign}(\eta_0) - \dot{d}. \end{cases} \tag{24}$$

Construct a Lyapunov function $V = \xi_e^\top P \xi_e$, where $\xi_e^\top = [|\eta_0|^{\frac{1}{2}}\text{sign}(\eta_0), \eta_1]$. According to [17], if the observer gains k_0, k_1 and the matrices P and Q_R of the Lyapunov function are appropriately selected, $V(x)$ is a quadratic and strict Lyapunov function satisfying

$$\dot{V}(t) \leq -|\eta_0|^{-\frac{1}{2}} \xi_e^\top Q_R \xi_e. \tag{25}$$

By means of Bihari's inequality, the decay of $V(x)$ satisfys

$$V(t) \leq \left(V^{\frac{1}{2}}(0) - \frac{\lambda_{\max}(P)}{2\lambda_{\min}^{\frac{1}{2}}(P)\lambda_{\min}(Q_R)} t \right)^2. \tag{26}$$

Moreover, the error system (24) will converge to zero in a finite time smaller than T_s

$$T_s = -\frac{2}{\sigma} V^{\frac{1}{2}}(0), \sigma = \frac{2\lambda_{\min}^{\frac{1}{2}}(P)\lambda_{\min}(Q_R)}{\lambda_{\max}(P)}. \tag{27}$$

Since the proposed Lyapunov function is an absolutely continuous function of η_0 and η_1, and it's positive definite and radially unbounded:

$$\lambda_{\min}(P)||\xi_e||_2^2 \leq V(x) \leq \lambda_{\max}(P)||\xi_e||_2^2 \tag{28}$$

where $||\xi_e||_2^2 = |\eta_0| + \eta_1^2$ is the Euclidean norm of ξ_e. Further analysis leads to

$$|\eta_1(t)| \leq \frac{V^{\frac{1}{2}}}{\lambda_{\min}^{\frac{1}{2}}(P)} \leq \frac{V^{\frac{1}{2}}(0) - \frac{2}{\sigma}t}{\lambda_{\min}^{\frac{1}{2}}(P)}. \tag{29}$$

Then, the robust CBF constrains (23) for IBVS system can be designed as

$$\begin{aligned} \boldsymbol{v}_c(\boldsymbol{s}) \in \{\boldsymbol{v}_c \in \mathbb{R} \,|\, & L_{g_1} h_i(\boldsymbol{s}) \boldsymbol{v}_c + L_{g_2} h_i(\boldsymbol{s}) \hat{\boldsymbol{d}} \\ & + \alpha(h_i(\boldsymbol{s})) \geq L_{g_2} h_i(\boldsymbol{s}) \rho(t)\} \end{aligned} \tag{30}$$

where $\rho(t)$ is a piecewise function given by

$$\boldsymbol{\rho}(t) = \begin{cases} \frac{V^{\frac{1}{2}}(0) - \frac{2}{\sigma}t}{\lambda_{\min}^{\frac{1}{2}}(P)}, & t \in [0, T_s] \\ \varepsilon, & t \in (T_s, +\infty). \end{cases} \tag{31}$$

Based on the analysis above, it is evident that $\boldsymbol{\rho}(t) \geq \hat{\boldsymbol{d}} - \boldsymbol{d}$. From Lemma 1, it can be derived that when the control input satisfies (30), the state $\boldsymbol{s}(t)$ will always remain within the safe domain Ω_s.

D. Safety-Critical Predictive Controller Design

To rigorously ensure system safety while maintaining the nominal controller's performance objectives, this paper develops a non-linear optimization framework:

$$\begin{aligned} \boldsymbol{v}^\star = \arg\min_{\boldsymbol{v}} \ & \|\boldsymbol{v} - \boldsymbol{v}_{\text{nom}}\|^2 \\ \text{s.t.} \quad & L_{g_1} h_i(\boldsymbol{s}) \boldsymbol{v} + L_{g_2} h_i(\boldsymbol{s}) \hat{\boldsymbol{d}} + \alpha(h_i(\boldsymbol{s})) \geq L_{g_2} h_i(\boldsymbol{s}) \rho(t). \end{aligned} \tag{32}$$

By minimizing deviations between the implemented control input and the nominal input, and rigorously enforcing safety conditions derived from CBFs via linear inequality constraints, this non-linear optimization framework establishes a provable equilibrium between safety guarantees and control performance.

V. Simulation Results and Discussion

In this section, some simulations are performed to verify the validity and performance of the proposed controller, and the results are compared with the MPC-CBF controller. The simulations comprise three tasks: static visual servoing with an obstacle, dynamic visual servoing for tracking a target object without obstacles and dynamic visual servoing for tracking a target object with an obstacle.

A. Simulation Configuration

The simulation environment in this study is established on the Ubuntu 20.04 operating system, integrating the Gazebo 11 physics engine and the ROS Noetic framework. A picture of the setup is shown in Fig. 1 The official UR5 robotic arm model is loaded with calibrated dynamic parameters, including six revolute joints and associated actuator and sensor plugins. A virtual Intel RealSense D415 camera model is mounted on the UR5 end-effector to track a 0.01 m × 0.01 m ArUco marker (ID=25) placed within the Gazebo scene. Real-time ArUco marker detection is achieved via the ROS aruco_ros package for image processing. The controller, developed in MATLAB/Simulink, leverages the ROS Toolbox to enable real-time communication with ROS, facilitating bidirectional data exchange of joint states and control commands between the simulation and the control system.

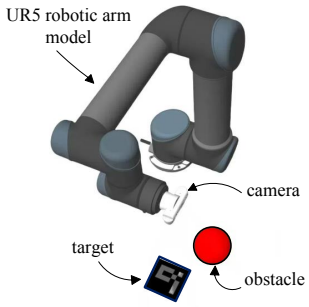

Fig. 1. Simulation configuration of visual servoing.

B. Application in Static Visual Servoing Tasks

This simulation investigates the performance of constrained visual servoing control in static scenarios where both the target and obstacle remain stationary. Fig. 2 presents temporal snapshots of the camera's FOV under the proposed safety-critical predictive control (ScPC) during static task execution, with subfigures (a)-(d) corresponding to initial configuration, intermediate operational states, and converged steady-state conditions, respectively. The simulation results are shown in Fig. 3, the proposed controller demonstrates faster target tracking convergence capability compared to the MPC method, with its error convergence curve exhibiting smoother characteristics.

Although both methods ultimately achieve comparable steady-state accuracy, the proposed ScPC shows superior energy efficiency during the control process. This is manifested through smaller control input adjustments, effectively

avoiding the frequent abrupt changes in control magnitude observed in the MPC approach. Both controllers successfully prevent target occlusion (Figs. 3(b) and (d)) via the CBF mechanism, validating their robustness in maintaining visibility constraints.

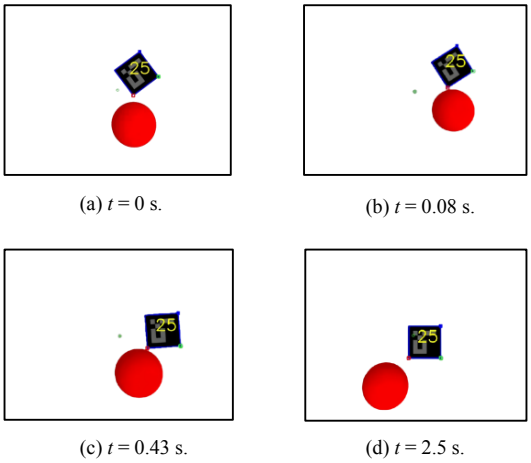

(a) $t = 0$ s. (b) $t = 0.08$ s. (c) $t = 0.43$ s. (d) $t = 2.5$ s.

Fig. 2. Camera images of ScPC under static visual servoing tasks.

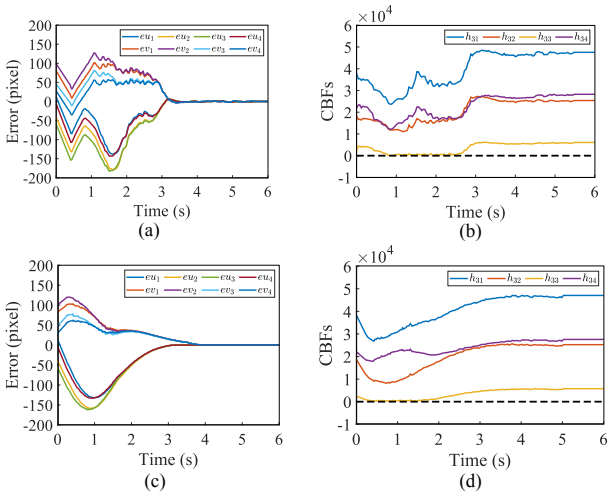

Fig. 3. Simulations results under static visual servoing tasks. (a) Tracking error curves $\boldsymbol{e}_s(t)$ of MPC-CBF. (b) Occlusion-free CBF constraints evolution $h_3(\boldsymbol{s})$MPC-CBF. (c) Tracking error curves $\boldsymbol{e}_s(t)$ of ScPC. (d) Occlusion-free RCBF constraints evolution $h_3(\boldsymbol{s})$ of ScPC.

C. Application in Dynamic Visual Servoing Tasks

This section evaluates the controller's performance under two dynamic scenarios where the target's motion is predefined but completely unknown to the control system. The experiments are designed to validate the controller's ability to handle unmodeled target kinematics while maintaining tracking precision and safety constraints.

Scenario A: Unobstructed Tracking with Unknown Motion. The target maintains a constant velocity of $\boldsymbol{v}_t = [0, 0.05, 0]^\top$ m/s during the time interval $t \in [0,3]$ s, with an intentionally introduced significant initial pose deviation between the system state and desired target configuration. As demonstrated in Fig. 4, comparative results reveal that the conventional MPC controller exhibits persistent steady-state errors during the disturbance phase ($t \in [0, 1.5]$ s). In contrast, the proposed predictive controller achieves precise tracking at $t = 1.5$ s.

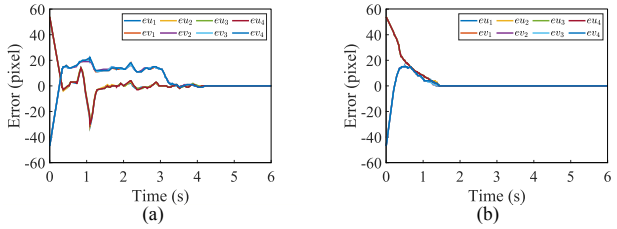

Fig. 4. Simulations results under dynamic visual servoing tasks without obstacle. (a) Tracking error curves $\boldsymbol{e}_s(t)$ of MPC-CBF. (b) Tracking error curves $\boldsymbol{e}_s(t)$ of ScPC.

Scenario B: Occlusion-Prone Navigation with Time-Varying Disturbances. Under identical kinematic parameters but with ideal initial state alignment, a spherical obstacle (0.01 m radius) induces feature loss during target motion. As shown in Fig. 5, the MPC-CBF method suffers control interruption at $t = 0.08$ s due to partial occlusion of the ArUco marker and subsequent feature point loss. In contrast, the proposed methodology maintains operational continuity.

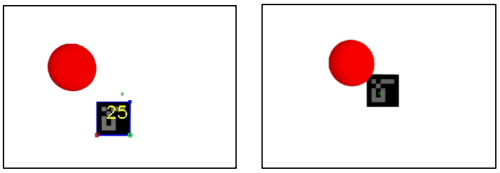

(a) $t = 0$ s. (b) $t = 0.08$ s.

Fig. 5. Camera images of MPC-CBF under dynaic visual servoing tasks with obstacle.

The efficacy of the ScPC method is demonstrated in Fig. 6(a) reveals the error convergence trajectory, and Fig. 6(b) illustrates the temporal evolution of the RCBF constraint $h_3(\boldsymbol{s})$, which maintains $h_3(\boldsymbol{s}) > 0$ throughout the operation. In particular, the obstacle exits the camera's field of view at $t = 0.98$ s, allowing full recovery of visual features while preserving safety guarantees.

Fig. 7 provides multitemporal visual evidence of the controller's robustness through sequential camera views. At $t = 0$ s, the system maintains stable initial tracking with complete marker visibility. During active obstacle avoidance at $t = 0.08$ s, partial occlusion is successfully managed without feature loss. The obstacle fully exits the FOV by $t = 0.98$ s, enabling immediate recovery of tracking accuracy, which stabilizes to steady state performance by $t = 1.68$ s.

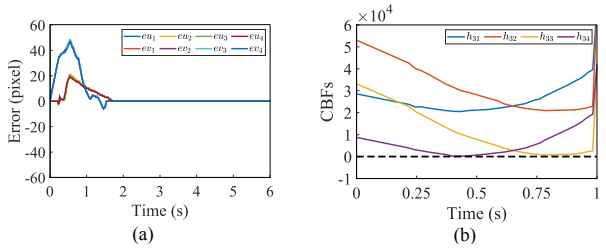

Fig. 6. Simulations results of ScPC under dynamic visual servoing tasks with obstacle. (a) Tracking error curves. (b) Occlusion-free RCBF constraints evolution $h_3(\boldsymbol{s})$.

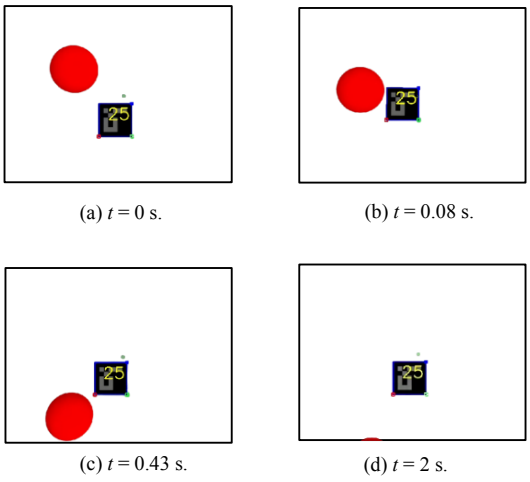

(a) $t = 0$ s. (b) $t = 0.08$ s.

(c) $t = 0.43$ s. (d) $t = 2$ s.

Fig. 7. Camera images of ScPC under dynamic visual servoing tasks with obstacle.

VI. Conclusion

This paper has presented a safety-critical predictive control framework for IBVS systems operating in dynamic environments with visibility constraints. By integrating RCBFs with generalized predictive control, the proposed methodology has addressed two critical challenges in visual servoing: (1) the accurate tracking of targets with unknown motion under disturbances, and (2) guaranteed visibility maintenance during occlusion events. The key innovations have been in the development of a nonlinear optimization framework that systematically reconciles control performance objectives with safety constraints through disturbance-adaptive barrier functions.

Future work will focus on extending the framework to multi-obstacle environments and validating performance on physical robotic platforms. Additional research directions include integration with learning-based perception systems and investigation of distributed implementation strategies for collaborative robotic tasks.

References

[1] T. Li, J. Yu, Q. Qiu, and C. Zhao, "Hybrid uncalibrated visual servoing control of harvesting robots with rgb-d cameras," *IEEE Transactions on Industrial Electronics*, vol. 70, no. 3, pp. 2729–2738, 2022.

[2] S. Kamtikar, S. Marri, B. Walt, N. K. Uppalapati, G. Krishnan, and G. Chowdhary, "Visual servoing for pose control of soft continuum arm in a structured environment," *IEEE Robotics and Automation Letters*, vol. 7, no. 2, pp. 5504–5511, 2022.

[3] F. Chaumette and S. Hutchinson, "Visual servo control. i. basic approaches," *IEEE Robotics & Automation Magazine*, vol. 13, no. 4, pp. 82–90, 2006.

[4] Q. Liu, J. Mao, L. Han, C. Zhang, and J. Yang, "Predictive observer-based dual-rate prescribed performance control for visual servoing of robot manipulators with view constraints," *IEEE Transactions on Cybernetics*, 2025.

[5] G. Wang, J. Qin, Q. Liu, Q. Ma, and C. Zhang, "Image-based visual servoing of quadrotors to arbitrary flight targets," *IEEE Robotics and Automation Letters*, vol. 8, no. 4, pp. 2022–2029, 2023.

[6] J. Lin, Z. Miao, H. Zhong, W. Peng, Y. Wang, and R. Fierro, "Adaptive image-based leader–follower formation control of mobile robots with visibility constraints," *IEEE Transactions on Industrial Electronics*, vol. 68, no. 7, pp. 6010–6019, 2020.

[7] Z. Miao, H. Zhong, J. Lin, Y. Wang, Y. Chen, and R. Fierro, "Vision-based formation control of mobile robots with fov constraints and unknown feature depth," *IEEE Transactions on Control Systems Technology*, vol. 29, no. 5, pp. 2231–2238, 2020.

[8] T. Zhu, J. Mao, L. Han, C. Zhang, and J. Yang, "Real-time dynamic obstacle avoidance for robot manipulators based on cascaded nonlinear mpc with artificial potential field," *IEEE Transactions on Industrial Electronics*, vol. 71, no. 7, pp. 7424–7434, 2023.

[9] J. Liu, J. Gao, W. Yan, Y. Chen, and B. Yang, "Image-based visual servoing of underwater vehicles for tracking a moving target using model predictive control with motion estimation," *International Journal of Vehicle Design*, vol. 91, no. 1-3, pp. 46–66, 2023.

[10] J. Gao, X. Liang, Y. Chen, L. Zhang, and S. Jia, "Hierarchical image-based visual serving of underwater vehicle manipulator systems based on model predictive control and active disturbance rejection control," *Ocean Engineering*, vol. 229, p. 108814, 2021.

[11] J. Lin, Y. Wang, Z. Miao, S. Fan, and H. Wang, "Robust observer-based visual servo control for quadrotors tracking unknown moving targets," *IEEE/ASME Transactions on Mechatronics*, vol. 28, no. 3, pp. 1268–1279, 2022.

[12] J. Yang, W. X. Zheng, S. Li, B. Wu, and M. Cheng, "Design of a prediction-accuracy-enhanced continuous-time mpc for disturbed systems via a disturbance observer," *IEEE Transactions on Industrial Electronics*, vol. 62, no. 9, pp. 5807–5816, 2015.

[13] A. D. Ames, J. W. Grizzle, and P. Tabuada, "Control barrier function based quadratic programs with application to adaptive cruise control," in *53rd IEEE Conference on Decision and Control*. IEEE, 2014, pp. 6271–6278.

[14] Y. Zhang, Y. Yang, and W. Luo, "Occlusion-free image-based visual servoing using probabilistic control barrier certificates," *IFAC-PapersOnLine*, vol. 56, no. 2, pp. 4381–4387, 2023.

[15] S. Wei, B. Dai, R. Khorrambakht, P. Krishnamurthy, and F. Khorrami, "Diffocclusion: Differentiable optimization based control barrier functions for occlusion-free visual servoing," *IEEE Robotics and Automation Letters*, 2024.

[16] Z. Jian, Z. Yan, X. Lei, Z. Lu, B. Lan, X. Wang, and B. Liang, "Dynamic control barrier function-based model predictive control to safety-critical obstacle-avoidance of mobile robot," in *2023 IEEE International Conference on Robotics and Automation (ICRA)*. Ieee, 2023, pp. 3679–3685.

[17] A. Levant, "Higher-order sliding modes, differentiation and output-feedback control," *International journal of Control*, vol. 76, no. 9-10, pp. 924–941, 2003.

[18] J. A. Moreno and M. Osorio, "Strict lyapunov functions for the super-twisting algorithm," *IEEE Transactions on Automatic Control*, vol. 57, no. 4, pp. 1035–1040, 2012.